

CEPHEID VELOCITY CURVES FROM LINES OF DIFFERENT EXCITATION AND IONIZATION. I. OBSERVATIONS

R. PAUL BUTLER¹

Astronomy Department, University of Maryland, College Park, MD 20742

Received 1992 November 20; accepted 1993 March 24

ABSTRACT

Radial velocity curves have been obtained from several hundred optical absorption lines for FF Aql, δ Cep, η Aql, and X Cyg. An iodine absorption cell has been used to reduce relative radial velocity errors to a few hundred meters per second. The shape and amplitude of the resulting radial velocity curves are in good agreement with previous results, particularly δ Cep which is shown to have been extremely constant over most of the last century. Velocities from atoms in low excitation potential (EP) levels (Fe I, Fe II, Sc II, Y II, Ti II) show positive velocity residuals of as much as 5 km s⁻¹ compared to high EP Fe I lines during the phase of rapidly decreasing velocity. The 8.12 eV line of Si II at 6348 Å has a negative velocity residual during the same phase. The asymmetry of the high EP Fe I, Ti II, and the Si II lines are similar and greater than the asymmetry of the low EP Fe I, Fe II, Sc II, and Y II lines.

Subject headings: Cepheids — stars: oscillations

1. INTRODUCTION

The radial velocity variability of δ Cep was first reported in 1895 by Belopolsky. Improving spectrographic technology over the last century has steadily revealed more intricate detail both in line profile variations and in the radial velocity curves of classical Cepheids. Observations of line doubling, line asymmetries, and line level effects provide valuable clues about the physical conditions in the pulsating atmospheres of Cepheids. Variations in color and radial velocity provide information about their radii and distances via the Barnes-Evans or Baade-Wesselink (hereafter BE/BW) method.

Emission lines and line splitting (\equiv line doubling) have been observed in Population II Cepheids by Joy (1939) and Sanford (1952). Kraft (1956) first reported similar line doubling behavior in the classical 16 day Cepheid X Cyg. More recently, line splitting in the infrared has been observed in the shorter period Cepheid X Sgr (Sasselov, Lester, & Fieldus 1989). This phenomenon indicates that strong shock waves propagate through the photospheres of moderate- and long-period Cepheids. Line doubling of H α has been reported in several long-period Cepheids (Grenfell & Wallerstein 1969; Wallerstein 1972, 1983).

Line asymmetries were observed in the long-period Cepheids T Mon and SV Vul by Sanford (1956), and in shorter period Cepheids by Sasselov et al. (1989). The asymmetries, when present, typically cause a redward displacement of the line core (Kraft 1956). In constructing a hydrodynamic model of a Cepheid atmosphere, Karp (1975) has shown that the asymmetry of weak lines is consistent with simple pulsational projection effects (Kulander & Jefferies 1966), but the asymmetry of strong lines requires a significant velocity gradient (Bell & Rodgers 1964; Sasselov & Lester 1990).

For 70 years observers have searched for evidence of line level effects in Cepheids, with limited success. Sanford (1956) found definitive evidence for differential velocities among lines in the long-period Cepheids T Mon and SV Vul. Lines of hydrogen, Sr II, and Ti II showed positive residuals of 10 to 60 km s⁻¹ compared to Fe I lines. This effect was primarily seen

during the cycle of rapidly decreasing velocity. Sanford did not find significant differences between lines of Fe I and Fe II. In a study of X Cyg, Abt (1978) compared the velocity curve obtained from 25 moderate and weak metal lines against that obtained from the strong lines of Sr II (4215 Å) and Ca I (4226 Å). The amplitude of the strong line velocity curve was approximately 10 km s⁻¹ greater than that due to the moderate and weak lines. Wallerstein and collaborators have reported a negative velocity residual for the 8.12 eV line of Si II at 6348 Å for several long-period Cepheids including X Cyg (Wallerstein 1983, 1972; Grenfell & Wallerstein 1969).

Evidence for line level effects in shorter period Cepheids has been much harder to detect. In a detailed study of δ Cep, Shane (1958) examined 116 blue lines “due to a variety of elements” but did not find significant evidence for differential velocities. Rodgers & Bell (1964) were unable to find velocity differences between Fe I and Fe II lines in β Dor. In a study of 40 red lines (including lines of Fe I, Fe II, Ca I, Sc II, Ba II, and Si II), no significant velocity differences were found for δ Cep or η Aql (Wallerstein 1979; Jacobsen & Wallerstein 1981). The amplitude of the H α velocity curve has been shown to be 20 to 100 km s⁻¹ greater than that due to metallic absorption lines for both short- and long-period Cepheids (Grenfell & Wallerstein 1969; Wallerstein 1972, 1979; Jacobsen & Wallerstein 1981; Wallerstein 1983).

The BE/BW method provides an observationally independent means of determining the radius and distance of a Cepheid (Wesselink 1946, 1969; Barnes, Evans, & Parsons 1976; Barnes et al. 1977). It thus serves as an important check on theoretically and empirically determined period-luminosity (-abundance-color) relationships. Historically it has been assumed that the motion of the continuum-forming region is accurately reflected by the radial velocity curve (along with a suitable pulsation factor). This is the equivalent of assuming either that the observed absorption lines are also formed in the continuum-forming region, or that outer atmosphere (roughly from $\tau = 1$ to $\tau = 0.1$) is comoving (Latyshev 1966; Manduca & Bell 1981; Böhm-Vitense et al. 1989). Errors in deriving Cepheid distances from BE/BW techniques are estimated to be in the range of from 10% to 20% (Karp 1975; Barnes et al.

¹ Current address: Astronomy Department, University of California, Berkeley, Berkeley, CA 94720. Electronic mail: paul@further.berkeley.edu.

1977; Sasselov & Lester 1990) up to 50% (Ferne 1984). Photometric errors and uncertainties in the temperature-color calibration are responsible for some part of this.

This study reports on four bright Cepheids, three of which have multiple period coverage. Observations have been made with a moderately high resolution ($\lambda/\Delta\lambda = 40,000$) echelle spectrograph that provides 1000 Å of coverage. The use of an iodine absorption cell has significantly improved the precision of radial velocity measurements by providing a fiducial wavelength scale and a means of extracting the instrumental point-spread function (PSF) directly from the observations. Evidence is presented of line level variations as a function of phase within the pulsating atmospheres of these Cepheids. A subsequent paper will attempt to understand the observed line level variations by kinematically imposing a variety of velocity gradients on synthetically generated spectra. Section 2 of this paper will cover the observations and reduction. Section 3 will compare the radial velocity results from this study with previous studies. Section 4 will report on line asymmetries and their effect on radial velocity measurements. Line doubling effects will appear in § 5, and line level effects will be covered in § 6.

2. OBSERVATIONS AND REDUCTION

All the observations reported in this paper were taken at Lick Observatory with the 0.6 m Coudé Auxiliary Telescope (CAT) and the "Hamilton" spectrograph. The "Hamilton" is a cross dispersed coude echelle spectrometer (Vogt 1987) that is currently fitted with a TI 800 × 800 CCD. A single image gathers 50 orders; each order is approximately 40 Å long. About 20 Å of spectrum is lost (goes undetected) between each order. The dispersion is 0.05 Å per pixel, and the FWHM of the instrumental profile is 2.5 pixels.

Observations of the stars listed in Table 1 were made over the 19 night span of 1990 August 14 to September 1 by the author. Exposure length varied from 1800 to 3600 s and yielded a typical signal-to-noise ratio (S/N) of 50 to 150. An exposure meter was used to determine the photon weighted mid-time of each exposure. The bright main-sequence dwarf HR 509 (G8 V) was observed throughout the observing run as a check on the intrinsic precision of the iodine absorption cell technique. The raw echelle images were converted to spectra with a customized "Hamilton" reduction package written primarily by G. Bari, G. W. Marcy, and J. A. Valent.

Traditional methods of measuring stellar radial velocities are seldom more accurate than 1 km s⁻¹. Griffin & Griffin (1973a) pointed out that instrumental errors could be eliminated if a reference spectrum were superposed on a stellar spectrum prior to the starlight entering the spectrograph. This has been attempted by a number of groups who have used telluric lines, chemical absorption cells, and Fabry-Perot interferometers to provide a reference spectrum (Griffin & Griffin

1973b; Campbell 1983; McMillan et al. 1993; Cochran, Hatzes, & Hancock 1991).

An iodine absorption cell has been chosen here over other options because of two important advantages: long-term stability and large wavelength coverage (5000 to 6200 Å). There are typically five or more iodine lines per angstrom throughout this entire range. The high density of iodine lines guarantees that every stellar line in an observation will be blended with two or more iodine lines. Over a period of 1.2 years Marcy & Butler (1992) have reduced radial velocity measurement errors of main sequence dwarf stars to 25 m s⁻¹ using the iodine absorption cell and the "Hamilton" spectrograph. Using the same observational setup described here (including the iodine cell), Butler (1992) has discovered the lowest amplitude Cepheid yet known. Further details about the choice of iodine and the construction of the cell are described in Marcy & Butler (1992).

The iodine absorption cell is mounted directly in front of the spectrograph slit. The cell operates as a transmission function on the incident starlight. Since the reference iodine spectrum is actually carried by the stellar beam as it passes through the spectrograph, it both records the effects of the PSF and provides a fiducial wavelength scale.

Two types of observations were made during the observing run. Approximately 10 "stellar template observations" and from 14 to 21 "stellar-iodine observations" were made of each of the four Cepheids in this program. A stellar-iodine observation was made with the iodine absorption cell in the telescope beam path. The resultant spectrum consists of the stellar spectrum multiplied by the iodine transmission function and convolved with the PSF. A stellar template observation consists of a normal observation of the star with the iodine cell removed from the beam path. The radial velocity information is contained within the stellar-iodine observations. The stellar template observations were used in a variety of tasks related to extracting the velocity information from the stellar-iodine observations. They also provide a record of the line profiles. Information about the stellar templates observations are given in Table 2, and the stellar-iodine observations are covered in Table 3. The phasing was determined from the ephemerides of Barnes, Moffett, & Slovak (1987). The S/N is a simple estimate of photon statistics.

Approximately 600 lines were identified in each of the four stars using a program to generate synthetic spectra (Bell 1973), a high-resolution solar atlas (Beckers, Bridges, & Gilliam 1976), and the US National Bureau of Standards solar wavelength table (Moore, Minnaert, & Houtgast 1966). Approximately 300 lines were judged to be reasonably free of blends and were further analyzed. Figure 1 shows a typical order of a δ Cep template spectrum.

The stellar-iodine observations were analyzed in three parts. First the iodine transmission function was recovered from each

TABLE 1
PROGRAM STARS

NAME	HR	HD	PERIOD (days)	MAGNITUDE		SPECTRAL RANGE
				Maximum	Minimum	
FF Aql	7165	176155	4.47	5.18	5.68	F5 Ia–F8 Ia
δ Cep	8571	213306	5.36	3.48	4.37	F5 Ib–G2 Ib
η Aql	7570	187929	7.17	3.48	4.39	F6 Ib–G4 Ib
X Cyg	7932	197572	16.38	5.87	6.86	F7 Ib–G8 Ib

TABLE 2
STELLAR TEMPLATE OBSERVATIONS

Star	JD + 2,440,000	Phase	Exposure Time (s)	S/N	
FF Aql	8117.769	995.112	3600	120	
	8123.757	996.452	2400	90	
	8124.718	996.667	2400	85	
	8125.743	996.896	2400	90	
	8126.766	997.125	2400	100	
	8127.766	997.348	2400	90	
	8134.702	998.900	1800	90	
	8135.709	999.125	2400	95	
δ Cep	8119.974	828.470	1800	135	
	8120.993	828.660	1800	135	
	8121.874	828.824	1800	120	
	8123.955	829.212	1800	165	
	8126.965	829.772	1800	125	
	8127.962	829.958	1800	170	
	8130.982	830.521	1800	140	
	8132.840	830.867	1800	120	
	8133.930	831.070	1800	175	
	8134.953	831.261	1800	150	
	8135.880	831.434	1800	140	
	η Aql	8117.870	661.646	2400	140
		8118.777	661.773	1800	120
8120.819		662.057	2400	205	
8125.774		662.748	2400	145	
8126.826		662.894	2400	205	
8130.737		663.439	2400	170	
8131.745		663.580	2400	140	
8133.761		663.860	2400	160	
8134.759		663.999	1800	185	
8135.768		664.140	2400	185	
X Cyg		8119.836	245.785	3600	65
	8120.885	245.849	3600	65	
	8124.900	246.094	3600	80	
	8125.959	246.159	3600	75	
	8127.913	246.278	3600	70	
	8130.865	246.458	3600	65	
	8133.880	246.642	3600	55	
	8134.882	246.703	3600	55	

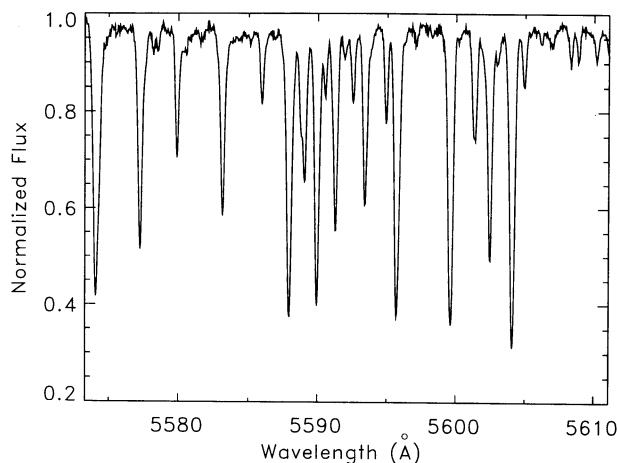


FIG. 1.—A representative example of the spectra obtained with the “Hamilton” echelle spectrograph. This spectrum is order 35 of δ Cep taken 1990 August 28.

point spread function of the FTS spectrograph is a delta function.

The “Hamilton” spectrograph PSF was determined with a non-near least-squares analysis that found the PSF which best mapped the FTS template iodine spectrum into the observed “Hamilton” iodine spectrum. A wavelength scale and an instrumental PSF were thus assigned to each stellar-iodine observation.

The Doppler shift of the stellar-iodine observation was then found with a modeling technique. The stellar template spectrum and the FTS iodine template spectrum were each given independent trial pixel shifts and then multiplied together. The product was then convolved with the Hamilton PSF determined from the previous step. Several of these “trial shift” models were made for each stellar-iodine observation. The stellar-iodine observation was then assigned the stellar and iodine pixel shifts of the model which best matched the observation, in a least-squares sense.

Since the iodine cell is stationary in the frame of the observer, the shift needed to match the template iodine to the observation is an instrumental effect. The true Doppler shift of the observation is thus the difference between the shift of the template stellar spectrum and the template iodine spectrum.

The intrinsic radial velocity precision of the iodine absorption cell together with the current generation of reduction and analysis software was determined by observing the stable main sequence dwarf HR 509 (G8 V) throughout the run. Reduction and analysis of the HR 509 spectra were done with the same software that was used for the Cepheids. The results are shown in Figure 2. The scatter in the velocities is just 0.021 km s^{-1} . The zero point in this figure is arbitrary. Since the line profiles of this star are stable, only a single stellar template observation was needed.

The phase-dependent change in the Cepheid line profiles makes it impossible to analyze all the stellar-iodine observations of a given Cepheid with a single Cepheid template spectrum. About 10 stellar template observations (no iodine) were therefore made of each Cepheid, at intervals of roughly 0.1 in phase. The position of each line in a Cepheid template spectrum was then determined in four ways. A parabola was fitted to the three lowest points in the line core (Nadeau & Millard

observation, then an instrumental PSF was determined, and finally a Doppler shift was assigned to each line. A detailed description of this analysis can be found in Marcy & Butler (1992).

Each stellar-iodine observation was paired up, by phase, with a stellar template observation. The iodine transmission function was recovered from each stellar-iodine observation by dividing out the stellar spectrum with the appropriate stellar template spectrum. Pixels affected by cosmic rays or poor stellar division were found by comparing the recovered iodine spectrum to an iodine spectrum taken the same night as the observation by shining an incandescent lamp through the iodine cell. Typically less than 2% of the pixels were judged to be bad, and they were subsequently avoided in the analysis. CCD pixels already known to be bad were also excluded from analysis.

The transmission function of the iodine absorption cell was determined at the McMath Solar Telescope using the Fourier Transform Spectrograph (FTS). The resolution of the FTS template iodine spectrum is 500,000 with a S/N of 1,000. The FTS spectrum carries an absolute, vacuum wavelength scale precise to one part in 10^8 . Relative to the “Hamilton,” the

TABLE 3
STELLAR-IODINE OBSERVATIONS

Star	Heliocentric JD + 2,440,000	Phase	Exposure Time (s)	S/N	Fe I Velocity (km s ⁻¹)	Star	Heliocentric JD + 2,440,000	Phase	Exposure Time (s)	S/N	Fe I Velocity (km s ⁻¹)	
FF Aql	8117.718	995.101	3600	100	-19.93	η Aql	8117.822	661.698	3600	155	6.96	
	8118.706	995.321	3600	75	-15.01		8118.752	661.827	2400	120	8.60	
	8119.746	995.554	3600	85	-5.40		8118.806	661.835	2400	125	6.55	
	8120.700	995.767	3600	90	-5.94		8118.896	661.847	2400	105	2.83	
	8121.694	995.990	1800	55	-18.62		8119.686	661.957	2400	165	-25.97	
	8123.729	996.445	2400	75	-9.36		8120.786	662.111	2400	160	-26.46	
	8123.825	996.467	2400	70	-8.59		8121.784	662.250	2400	95	-20.57	
	8124.686	996.659	2400	75	-3.68		8123.792	662.529	2400	140	-9.74	
	8124.784	996.681	2400	75	-3.66		8124.751	662.663	2400	135	3.25	
	8125.682	996.882	2400	80	-13.07		8125.713	662.797	2400	130	10.43	
	8125.807	996.910	2400	70	-15.01		8125.838	662.815	2400	120	9.16	
	8126.682	997.106	2400	85	-19.73		8126.712	662.936	2400	175	-22.34	
	8126.798	997.131	2400	80	-19.62		8126.866	662.958	2400	165	-26.05	
	8127.678	997.328	2400	75	-14.81		8130.710	663.493	2400	140	-11.90	
	8130.680	998.000	2400	85	-18.93		8130.769	663.502	2400	140	-11.44	
	8131.687	998.225	2400	70	-18.53		8131.717	663.634	2400	120	-0.03	
	8132.739	998.460	2400	70	-9.13		8132.683	663.768	2400	120	9.82	
	8133.708	998.677	2400	65	-3.90		8133.674	663.906	2400	140	-16.12	
	8134.676	998.893	2400	80	-13.18		8133.793	663.923	2400	145	-20.32	
	8134.791	998.919	2400	75	-14.98		8134.736	664.054	2400	175	-28.53	
8135.681	999.118	2400	80	-19.63	8135.741	664.194	2400	155	-22.96			
δ Cep	8117.993	828.100	1800	135	-28.34	X Cyg	8118.845	245.724	3600	45	36.33	
	8119.949	828.465	1800	110	-9.84		8119.791	245.782	3600	55	31.59	
	8120.969	828.655	1800	115	-0.28		8119.895	245.788	3600	50	30.06	
	8121.811	828.812	1800	95	5.86		8120.744	245.840	3600	50	21.57	
	8123.906	829.202	1800	135	-23.77		8120.933	245.852	3600	50	20.70	
	8124.985	829.403	1800	120	-13.22		8121.905	245.911	2600	40	17.29	
	8125.991	829.591	1800	105	-3.68		8124.819	246.089	3600	75	-15.42	
	8126.735	829.729	1800	110	4.47		8125.914	246.156	3600	60	-10.62	
	8126.984	829.776	1800	105	6.56		8126.930	246.218	3600	65	-4.59	
	8127.712	829.911	1800	140	-22.66		8127.829	246.273	3600	65	-0.02	
	8127.792	829.926	1800	150	-26.26		8130.805	246.454	3600	55	15.05	
	8127.875	829.942	1800	160	-28.86		8130.909	246.460	3600	50	15.68	
	8127.982	829.962	1800	135	-31.23		8133.831	246.639	3600	50	30.73	
	8130.957	830.516	1800	110	-7.01		8134.827	246.700	3600	50	35.74	
	8132.706	830.842	1800	115	1.04							
	8132.863	830.871	1800	110	-8.99							
	8133.731	831.033	1800	140	-31.29							
	8133.949	831.074	1800	145	-29.94							
	8134.929	831.256	1800	125	-20.97							
	8135.854	831.429	1800	115	-11.58							

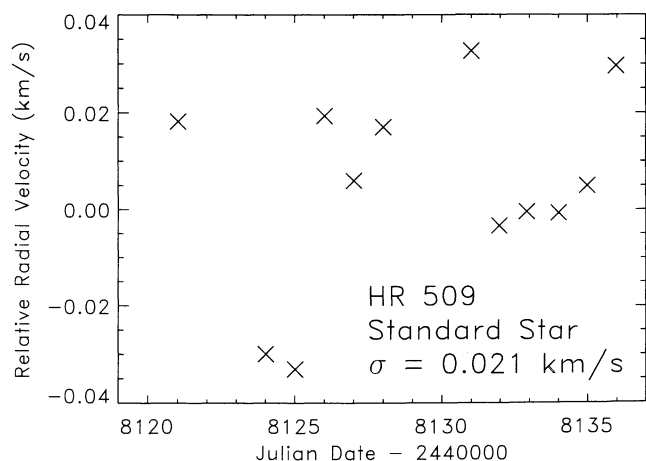


FIG. 2.—Radial velocity results for the reference star HR 509 (G8 V). The standard deviation of the velocity scatter is 0.021 km s⁻¹.

1988). A Gaussian was fitted to the line core. The 0.7 and 0.5 line bisectors (line core = 1, continuum = 0) were found by linear interpolation (Kulander & Jefferies 1966). As § 4 will demonstrate, the resulting radial velocity will critically depend on which technique is used to determine the line location. In each case the line position was determined only in the local unit of pixels. The pixel location of a stellar line in a stellar-iodine observation was then found by adding the stellar template line position to the stellar pixel shift found in the modeling process. Pixel locations were converted to wavelength based on the known wavelength of the FTS iodine spectrum.

The iodine absorption cell technique does not provide absolute radial velocities. The velocity zero point for all iodine observations is arbitrary. The advantage of using an iodine absorption cell is the improvement in the internal precision of the radial velocity measurements, thus making possible the search for differential effects. Pseudo-absolute velocities have been concocted by assigning a rest wavelength to each line. The rest wavelengths were taken from the US National Bureau

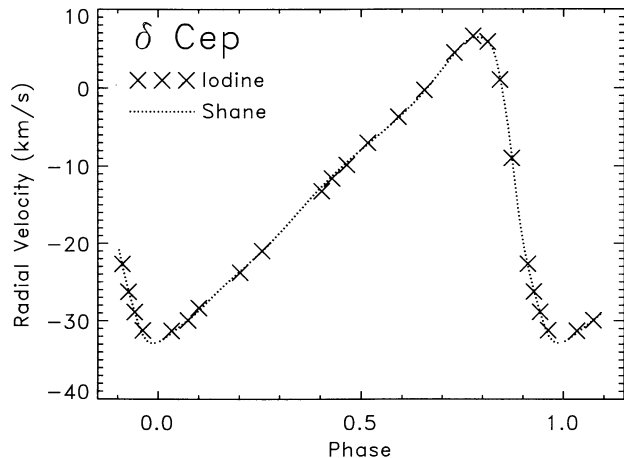


FIG. 3.—Radial velocity curve for δ Cep. The iodine velocities are the average of 53 strong high EP (3–6 eV) lines of Fe I. The iodine velocities were phased with the ephemeris of Barnes et al. (1987). The period of Shane's results were retarded by 0.1168, and a constant of 2.379 km s^{-1} has been added to the velocities to match the iodine results. The standard deviation of the differences between the two data sets is 0.289 km s^{-1} . The shape and amplitude of the δ Cep radial velocity curve has been remarkably constant over the last century.

of Standards solar wavelength table (Moore et al. 1966). No attempt has been made to correct for wavelength shifts due to pressure or gravitation or other effects. This has led to a systematic offset of 2.379 km s^{-1} between the stellar-iodine velocity set reported in this paper and previous studies (in particular Shane 1958). This systematic velocity shift has no effect on either the search for differential velocities or on the shape of the derived velocity curves.

3. RADIAL VELOCITY CURVES

A “standard” radial velocity curve for each of the program stars was constructed by averaging the results for about 50 strong, high EP (3–6 eV) Fe I lines. Line positions were determined with the 0.7 bisector method. The velocity results are given in Table 3 and shown in Figures 3–6. Table 4 provides a

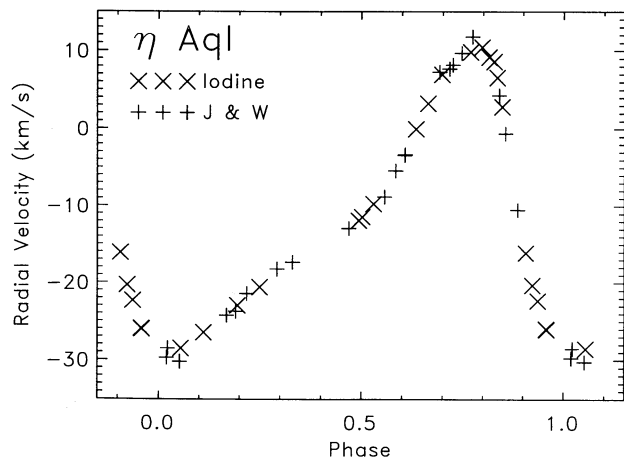


FIG. 4.—Radial velocity curve for η Aql. Both data sets were phased with the ephemeris of Barnes et al. (1987). A constant of 2.379 km s^{-1} was again added to J&W's results to match the iodine velocities. There is no evidence of a phase shift between the two data sets.

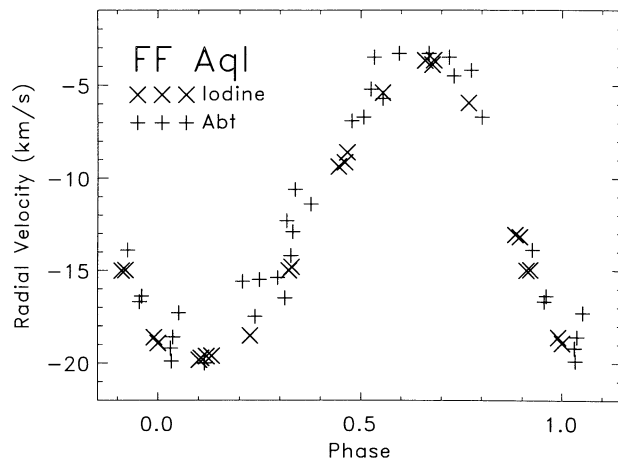


FIG. 5.—Radial velocity curve for FF Aql. A constant of 8.3 km s^{-1} was added to Abt's results. FF Aql is the primary member of a binary system, which probably accounts for the large velocity offset.

list of the high EP Fe I lines that were used to construct the “standard” velocity curves.

Of the stars in this program, δ Cep has been observed the most frequently and has the most precisely determined radial velocity curve. In particular, Shane (1958) has phased three data sets taken with a single spectrograph over a span of several decades (1907, 1923, 1950) at a resolution of 11 \AA mm^{-1} . Figure 3 shows the definitive radial velocity curve that Shane constructed by averaging almost 100 observations together. A constant of 2.379 km s^{-1} has been added to Shane's data set and the period has been retarded by 0.1168 to match the stellar-iodine velocities. The shape of Shane's velocity curve is remarkably similar to that given by the stellar-iodine velocities, which consist of 20 observations taken over three consecutive pulsation periods. Individual points differ typically by less than 0.3 km s^{-1} . This suggests that the shape and amplitude of δ Cep is extremely constant on time scales of a century. This is consistent with the long-term photometric study of Fernie (1992) which suggests that the amplitudes of Cepheids are stable on time scales of decades or more.

A total of 21 stellar-iodine observations of η Aql were taken over a span of two and one-half pulsation periods. Figure 4

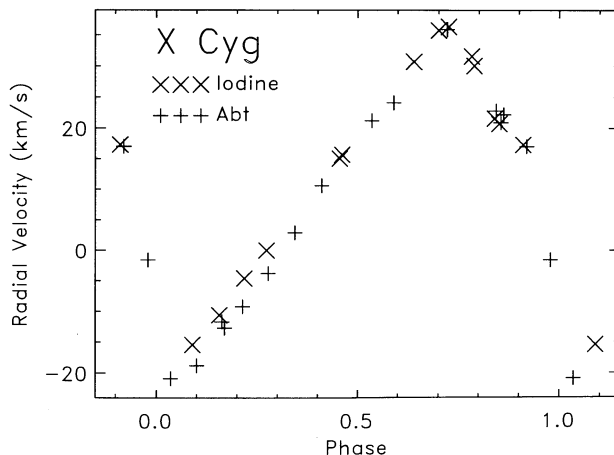


FIG. 6.—Radial velocity curve for X Cyg

TABLE 4
"STANDARD" Fe I LINES USED IN VELOCITY ANALYSIS

λ (Å)	EP (eV)	FF Aql	δ Cep	η Aql	X Cyg
5016.35	3.94	...	X	X	...
5040.67	3.36	X	X	X	...
5056.06	3.64	...	X	...	X
5092.21	4.25	X	X	X	X
5127.65	4.25	X	X	X	X
5135.11	4.17	X	X	X	X
5189.37	4.14	X	X
5192.92	3.03	X	X	X	X
5197.55	4.25	X	X
5229.85	4.22	X	X	X	X
5231.32	3.28	X	X	X	...
5243.96	3.63	X	X	X	X
5283.27	3.03	X	X	X	X
5290.01	3.69	X	X	...	X
5322.59	4.43	...	X
5325.66	3.21	X	X	X	X
5341.43	3.26	X	X	X	X
5368.95	4.41	X	X	X	X
5375.20	4.47	X	X	X	X
5381.08	3.69	X	X	...	X
5384.87	4.31	X	X	X	X
5390.98	4.41	X	X	X	X
5392.03	4.00	...	X
5392.97	4.15	X	X	X	X
5394.67	3.24	X	X	X	X
5425.58	4.32	X	X	X	X
5434.47	4.43	X	X
5446.55	4.38	...	X	X	...
5474.25	4.20	X	X
5475.43	4.15	X	X
5489.28	4.14	X	X	X	...
5534.28	3.57	...	X	...	X
5544.72	3.69	...	X	X	X
5545.47	4.21	X	X	X	X
5586.32	3.57	...	X	...	X
5588.31	3.36	X	X	X	X
5635.54	4.99	X	X	...	X
5639.84	4.22	X	X	X	X
5695.23	4.00	...	X	...	X
5707.57	4.60	X	X	X	...
5710.98	3.36	X	X
5753.64	4.54	X	X	...	X
5754.74	4.26	X	X	X	...
5764.59	4.20	X	X	X	X
5808.34	4.60	...	X	...	X
5810.85	3.88	...	X	...	X
5817.97	4.54	X	X	X	X
5931.82	4.65	X	X	X	X
5936.31	3.92	X	X	X	X
6004.69	3.88	X	X	X	X
6010.25	3.88	X	X	X	...
6057.67	4.73	...	X	X	X
6080.19	4.79	X	X	X	...
6129.61	4.14	X
6189.75	3.94	X
6273.03	3.33	X

compares the resulting stellar-iodine radial velocity curve to that of Jacobsen & Wallerstein (1981), which was again shifted by a constant velocity of 2.379 km s^{-1} . The resolution of the J&W observations is 10 Å mm^{-1} . The two data sets were phased together with the ephemeris of Barnes et al. (1987). No evidence of phase shift is observed between the two data sets. It is unfortunate that both data sets undersample the velocity curve near the secondary bump. The two data sets are in good agreement, though there is clearly less scatter within the stellar-iodine velocity set. In particular, the stellar-iodine

velocity data point near phase 0.95 is actually two velocity measurements. By coincidence these two data points were taken almost exactly one period apart, and they agree to within 0.08 km s^{-1} . In contrast, the Jacobsen & Wallerstein data scatter at the $1\text{--}2 \text{ km s}^{-1}$ level.

It has been reported that the IR radial velocity curves of Cepheids have a significantly greater amplitude than their optical counterparts (Sasselov et al. 1989; Sasselov & Lester 1990). The only star in common to the IR studies and this paper is η Aql. The full amplitude η Aql reported by Sasselov & Lester (1990) agrees with the results given in Table 3 of this paper to within 1 km s^{-1} . The IR velocity curve is unfortunately undersampled near maximum velocity.

There are surprisingly few high-quality radial velocity curves for either FF Aql or X Cyg. Figure 5 shows perhaps the finest set of photographic radial velocities ever taken for FF Aql (Abt 1959). The iodine velocity set is composed of 21 observations taken over four consecutive cycles. It was necessary to add a constant 8.3 km s^{-1} to Abt's velocities to match the iodine results. FF Aql is a member of a binary system, which probably accounts for the large velocity offset. The shape and amplitude of the two velocity curves agree to the limit imposed by scatter in the Abt data set.

Figure 6 compares the iodine radial velocity curve of X Cyg with that of Abt (1978). The Abt data set consists of 17 observations taken over three pulsation cycles in 1955. The iodine data set consists of 14 observations taken over just a single cycle. The two data sets were phased up with the ephemeris of Barnes et al. (1987). Though the two data sets were taken 35 years apart they have a very similar shape and amplitude. The Abt data show a slightly greater slope compared to the iodine along the rising branch of the radial velocity curve. There is no evidence for a phase shift. It is again unfortunate that both data sets undersample the curve near the secondary bump on the descending branch of velocity curve.

Measurement errors are estimated from a variety of sources. Within a single observation the velocity scatter of the "standard" high EP Fe I lines was typically 0.4 km s^{-1} . This is taken to be the precision of a single line. Averaging the velocities of 10 or more such lines improves the precision to 0.1 km s^{-1} for a single observation. This is in good agreement with the observed cycle-to-cycle consistency seen in the three program stars with multiple period coverage. The precision of the reference star, HR 509, is expected to be 3–5 times better than the Cepheids because of narrower absorption lines (Merline 1985). The precision of the X Cyg velocities are about a factor of 2 worse than δ Cep or η Aql because of lower S/N.

4. LINE ASYMMETRIES AND RADIAL VELOCITY

The extreme and rapidly changing asymmetry inherent in Cepheid absorption lines complicates the issue of assigning a position, and subsequently a velocity, to individual lines (Kraft 1967). A number of methods have been attempted including "mask" cross correlations (Barnes et al. 1987; Gieren 1981), line bisectors, and line core minima. Each of these methods suffers from a number of difficulties. Mask cross correlations do not work well for stars whose spectral type is undergoing large changes, and they are intrinsically unable to record the spectrum that is used to generate the velocity measurement. Techniques that find the line core minima or fit a symmetric function (e.g., Gaussian or Lorentzian) to the line profile are strongly affected by changing line profile asymmetries. The

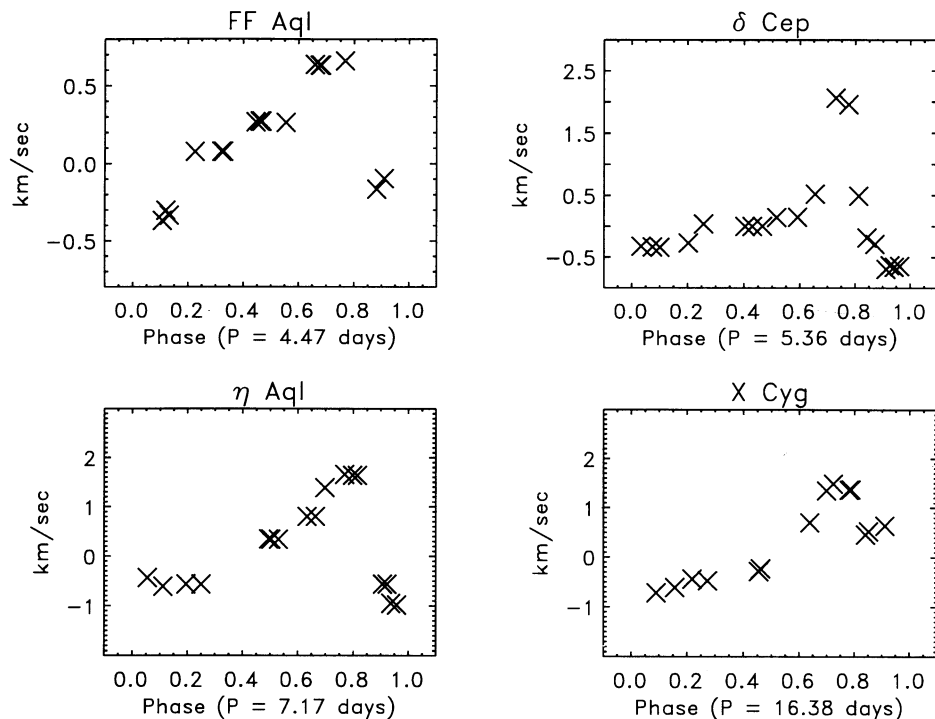


FIG. 7.—Difference between parabolic minimum radial velocity curve and 0.7 bisector radial velocity curve. The parabolic minimum technique for determining radial velocities is particularly sensitive to changing line asymmetries. The amplitude of the parabolic minimum radial velocity curves is from 1 to 3 km s^{-1} greater than those derived from the 0.7 bisector method.

problem with the line bisector technique depends on the bisector chosen. A 0.8 or 0.9 bisector will not be strongly affected by line blends, but it will be affected by changing line profile asymmetries. A 0.5 bisector will be relatively insensitive to changing line asymmetries in a Cepheid, but it will be affected by line blends.

The choice of radial velocity method will have a significant effect on the amplitude and shape of the velocity curve. This is demonstrated in Figure 7 which shows the radial velocity difference between the parabolic minimum technique and the 0.7 bisector method for each of the four program stars. The same set of “standard” high EP Fe I lines (Table 4) were used to generate the radial velocity curve for the 0.7 bisector and the parabolic minimum techniques; thus the radial velocity differences are entirely due to measurement technique differences. The difference between the two techniques changes most rapidly between phase 0.6 and 0.0, just before and during the time of velocity reversal. The three normal-amplitude Cepheids have a differential velocity “hump” near phase 0.8, while the small-amplitude Cepheid, FF Aql, shows only a simple linear trend from phase 0.0 to 0.8. Compared to the 0.7 bisector method the amplitude of the radial velocity curve from the parabolic minima technique is larger by 5%–6% for FF Aql and δ Cep, and 7%–8% for η Aql and X Cyg.

The reason for this is illustrated in Figure 8 which shows how the line profile for a strong high EP Fe I line changes as a function of phase for η Aql. The Doppler shift differences between phases have been removed, and each line has been plotted with the line core minima at 0 km s^{-1} . The line profiles are reasonably symmetric from phase 0.2 to 0.6. From phase 0.6 through 0.8 the line core is seen to be displaced redward relative to the line wings. From phase 0.85 through 0.14 the

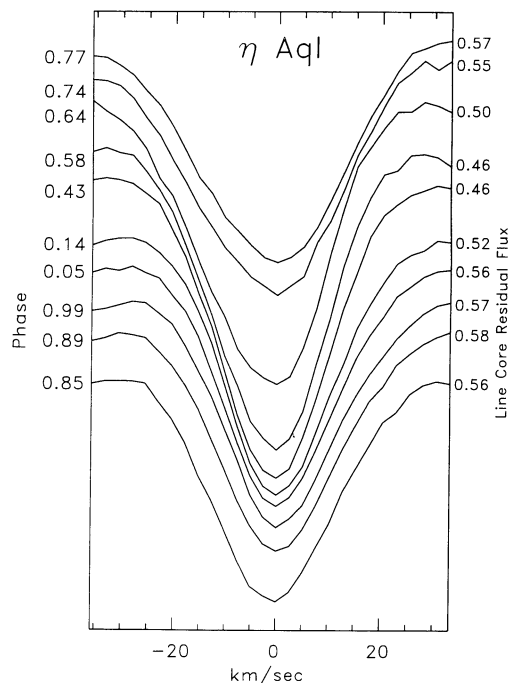


FIG. 8.—Line profile variations as a function of phase for the strong Fe I line (5135 \AA , 4.17 eV) in the spectrum of η Aql. The profiles have been shifted horizontally so that the line core minima are centered at 0 km s^{-1} . The profiles have also been shifted vertically by an arbitrary amount. From phase 0.2 through 0.6 the line profiles are reasonably symmetric. From phase 0.6 through 0.8 the line core is strongly redshifted relative to the wings. From phase 0.85 through 0.14 the line core is blueshifted.

line core is displaced toward the blue relative to the wings. Because the parabolic minimum technique “sees” only the line core, it is very susceptible to line asymmetry variations.

Historically, a constant pulsation factor has been used to convert from radial velocity to pulsation velocity (Carroll 1928; Getting 1935). Within the last 20 years more sophisticated attempts have been made to consider how the pulsation factor is affected by the method used to measure radial velocity (Parsons 1972; Hindsley & Bell 1986). The implicit assumption is still made that for a given star and a given radial velocity technique, a constant pulsation factor can be used to convert from radial velocity to pulsation velocity. As Figures 7 and 8 demonstrate, this is not strictly true. From phase 0.2 to 0.6 the line profiles are reasonably symmetric, and almost any technique used to assign line position will give comparable results to within 0.5 km s^{-1} . It is unfortunately during the phase of velocity reversal, when the Cepheid is going through both its maximum and minimum velocity, that different techniques give significantly different and nonlinear results. The determination of a pulsation factor must therefore take into account not only what technique is used to measure radial velocity, but also how changing line asymmetries affect the radial velocity measurement as a function of phase. The pulsation factor thus cannot be a constant; it must also be a function of phase. Section 6 will show that the pulsation factor is also a function of the particular set of lines from which the radial velocity information is extracted.

Based on a hydrodynamic model of a classical 12 day Cepheid, Karp (1975) has shown that the pulsation factor is a function of line width and of measurement method, particularly for the case of weak lines using the line minima technique. In contrast, the pulsation factor of strong lines measured with the 0.5 bisector method were insensitive to line width variations. Karp strongly advocates the use of a 0.5 bisector to measure radial velocities. Karp of course had the advantage of being able to synthesize isolated lines. Unfortunately, spectral regions that contain significant amounts of radial velocity information also have significant line-blending problems, as shown in Figure 1. As the line bisector moves further into the wings of a line, the problem of line blending increases, and the number of usable lines decreases. For this reason, it is desirable to use a line bisector somewhat nearer the line core.

A 0.7 bisector was chosen because it has given good results for previous observers and it gives excellent agreement with photographic results, as demonstrated in Figures 3 through 6. This last point cannot be stressed too heavily. Photographic results will constitute the majority of the historic radial velocity record for the next half century. To search for changes in the amplitude or shape of the radial velocity curve, it is necessary to choose a measurement technique that is influenced by line asymmetries in a way that is similar to the “eyeball and micrometer” measurements of the photographic era. A 0.7 bisector is consistent with Parsons (1972) who notes that the measured line center of photographic spectra is probably between a 0.5 and 0.8 bisector for both eyeball and Grant comparator machines.

It is well known that the quality of photographic radial velocities varies significantly from observer to observer. After a fairly extensive search of the literature, the author has concluded that photographic results shown in Figures 3 through 6 are among the very best of previously determined radial velocity curves for the Cepheids in this program. These observations were taken from roughly 1920 to 1980. The radial velocity

precision for the observations from the 1920s compare very favorably with the later observations.

5. LINE SPLITTING

Spectroscopic observations of line splitting in a pulsating star are usually interpreted as a dramatic manifestation of a shock wave passing through the line forming region of the atmosphere. Line doubling in the Population II Cepheid W Vir was first reported by Sanford (1952). From a series of blue spectroscopic observations, it was shown that many metal lines exhibited line splitting. Kraft (1956) reported that a small number of low-excitation lines ($< 1.23 \text{ eV}$) showed evidence of doubling in X Cyg.

Line splitting was first observed in a short-period Cepheid (X Sgr, $P = 7^d$) by Sasselov et al. (1989). Over a 300 \AA region near 1.1 \mu m they observed all of the photospheric lines to periodically undergo large asymmetries or to actually double near the phase of velocity reversal. Contrary to their expectations, line splitting was not observed in spectra taken near 1.6 \mu m (Sasselov & Lester 1990). In an attempt to understand this behavior they showed that an opacity bump existed near 1.1 \mu m , which caused lines to be formed higher in the atmosphere. Based on opacity bumps near 5300 and 6100 \AA , they suggest that line splitting might also be observed in the visible.

There are no unambiguous examples of line splitting in the region of 4800 to 6400 \AA for any of the program stars. Figure 9 shows a typical series of low EP Fe I line profiles for X Cyg. The profiles of the low EP Fe I lines remain fairly symmetric throughout the entire pulsation cycle. Kraft (1967) has noted that line doubling in X Cyg varies from cycle to cycle. It is possible that the observations reported in this Paper were made during a quiescent cycle, or perhaps line doubling does not occur in the green to orange spectral range.

It was not possible to recover the Na D line profiles because the interstellar D lines were superposed on the stellar D lines.

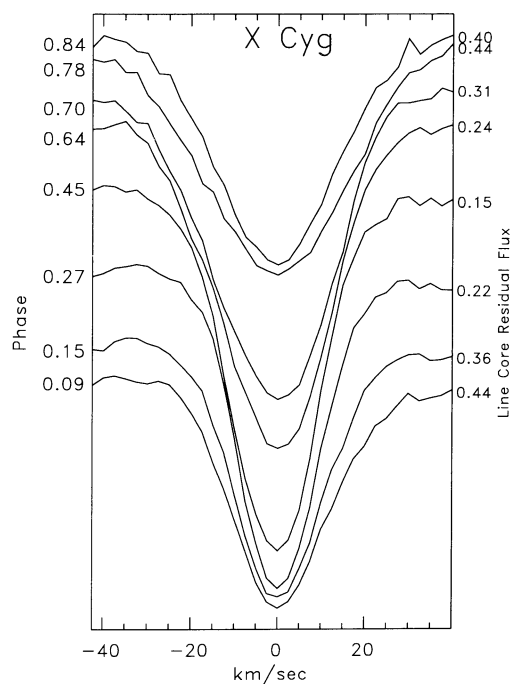


FIG. 9.—Same as Fig. 8 for the strong Fe I line at 5499 \AA (1.01 eV) in the spectrum of X Cyg.

6. LINE LEVEL EFFECTS

Radial velocity curves have been determined for seven classes of lines. Figures 3 through 6 show the velocities determined from Fe I lines with large excitation potentials (3–6 eV). Velocities derived from these lines have been designated as the “standard” because these lines are very numerous in the spectral window of this study. The other classes of lines include Sc II and Y II (0.5–1.5 eV), Ti II (1.0–2.0 eV), Fe I (0.5–2.4 eV), Si I and Mg I (4–6 eV), and the Si II line at 6348 Å (8.121 eV). The Si II line is formed at a deeper level in the atmosphere than the standard Fe I lines. The Si I and Mg I lines are probably formed near the region of the standard lines, and the other classes of lines are presumably formed at higher levels in the atmosphere. The standard high EP Fe I lines used in this study are listed in Table 4, and the rest of the lines are listed in Table 5.

Individual stellar lines were thrown out for a number of reasons. Weak lines were not used because they disappear for a fraction of the pulsation cycle and they are difficult to measure. Lines contaminated with nearby companion lines were also excluded. A line was omitted if the rms of the fit from the velocity modeling process described in § 2 was poor. Finally, all of the measurements of a given line were omitted if more than two observations of that line needed to be excluded.

Figures 10–13 show the residual velocities of each of the classes of lines relative to the standard Fe I lines. The results are reminiscent of Sanford’s study (1956) of the long-period Cepheids T Mon and SV Vul. As in Sanford’s study, the velocities of the various classes of lines typically differ from the standard lines only during the phase of velocity reversal. With the exception of the Si II line, the velocity residuals are primarily positive.

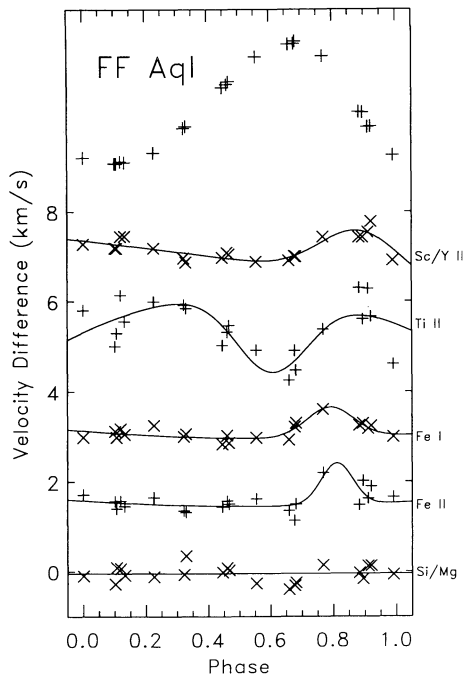


FIG. 10.—Residual radial velocities for various classes of lines in FF Aql. The standard velocities (shown at top and in Fig. 5) are from the high EP (3–6 eV) Fe I lines (Table 4). The residual velocities for a given class of lines are formed by subtracting the velocity curve of the standard high EP Fe I lines from the velocity curve of the given line class. The classes of lines are shown along the right edge and listed in Table 5. The Fe I residuals are from low EP lines. An arbitrary offset has been added to each of the line sets.

TABLE 5
ABSORPTION LINES USED IN VELOCITY ANALYSIS

Atom	λ (Å)	EP (eV)	FF Aql	δ Cep	η Aql	X Cyg
Y II	5088.84	1.08	X	X	X	X
Sc II	5241.28	1.45	X	X	X	X
Y II	5291.29	1.03	X	...	X	X
Sc II	5319.83	1.35	X	X	X	X
Sc II	5528.36	1.76	X	X	X	X
Y II	5547.56	1.74	X	...	X	X
Sc II	5642.55	1.50	X	X	X	X
Ti II	5187.35	1.88	X	X	X	X
	5338.30	1.57	X	X	X	X
	5382.52	1.56	X	X	X	X
	5420.29	1.57	X	X	X	X
Fe I	5013.47	0.85	X	X
	5051.23	2.27	X	X	...	X
	5084.76	0.95	X	X	X	X
	5128.79	0.91	X	...
	5143.18	2.42	X
	5146.53	2.19	X
	5173.04	1.48	X	X	X	X
	5196.39	1.55	X	X
	5226.99	0.11	X
	5271.00	1.97	X	X	...	X
	5323.53	2.27	...	X	...	X
	5342.52	1.60	X	X	X	X
	5431.21	2.20	X	X
	5436.04	2.32	X	X	...	X
	5499.05	1.01	...	X
	6215.16	2.22	X
	6254.29	2.40	X
	6255.99	2.27	X
	6258.10	2.45	X	X
	6266.88	2.17	X	X
Fe II	5199.02	3.23	...	X	X	...
	5236.09	3.22	X	X	X	X
	5318.10	3.15	X
	5327.04	3.22	X	X	X	X
	5339.21	3.23	X	X	X	X
	5426.77	3.20	X	X	X	...
	5536.39	3.24	X	X	X	X
	5993.04	3.15	X	...	X	X
Mg I	5174.14	6.24	X	X	X	X
Mg I	5185.05	6.25	X	X	X	X
Si I	5490.51	5.61	X
Mg I	5530.00	4.34	X	X	X	X
Si I	5647.18	4.93	X	X	...	X
Si I	5692.01	4.93	X	X	...	X
Mg I	5712.68	4.34	X	X	X	X
Si I	5773.75	5.08	X	X	...	X
Si I	5950.19	5.08	X	X	X	X
Si I	6126.72	5.61	...	X	X	X
Si I	6146.72	5.62	...	X	X	X
Si I	6196.13	5.87	X
Si I	6197.15	5.87	X
Si II	6348.86	8.12	...	X	X	X

The residual velocity results for FF Aql are plotted in Figure 10. FF Aql is a short-period Cepheid with a relatively small amplitude and an almost sinusoidal velocity curve. There is little evidence for differential velocities. None of the classes of lines differs from the standards by as much as 1 km s⁻¹. The velocity of the low excitation potential (EP) lines of Sc II and Y II go through a 0.5 km s⁻¹ residual hump from phase 0.75 through 0.95 relative to the high EP Fe I lines. In contrast, the Ti II lines seem to go through a 0.5 km s⁻¹ slump just before the velocity reversal. The slightly positive residual velocity of the Fe II lines and of the low EP Fe I lines is suggested

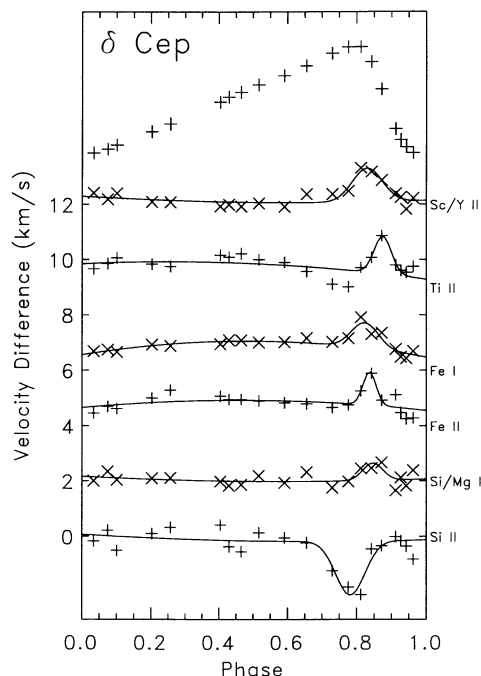


FIG. 11.—Same as Fig. 10 for δ Cep. The standard high EP Fe I velocity curve is shown at top and in Fig. 3.

only by a single observation ($P = 0.76$), and is therefore questionable. The high excitation Si I and Mg I lines do not differ from the standard Fe I lines at the level of 0.2 km s^{-1} . The 8.12 eV Si II line in several critical observations of FF Aql fell on a bad CCD column. It was therefore not possible to make velocity measurements of this line.

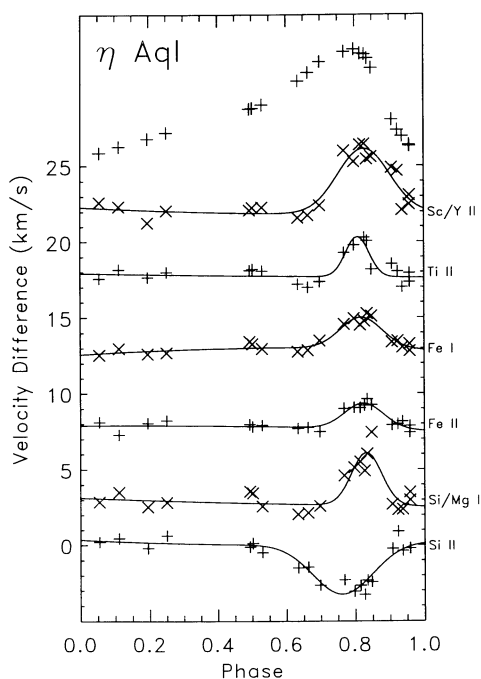


FIG. 12.—Same as Fig. 10 for η Aql. The standard high EP Fe I velocity curve is shown at top and in Fig. 4.

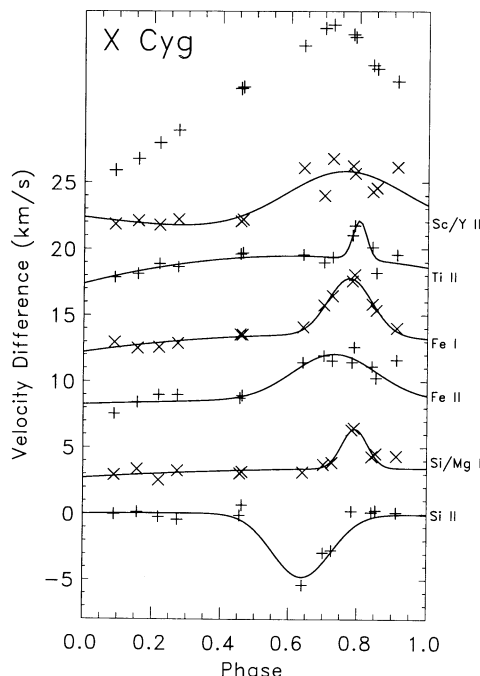


FIG. 13.—Same as Fig. 10 for X Cyg. The standard high EP Fe I velocity curve is shown at top and in Fig. 6.

The differential velocities for δ Cep are shown in Figure 11. While the effects are still small, they are certainly more obvious than the case of FF Aql. All four low excitation potential line sets show positive residual velocities at the $1\text{--}2 \text{ km s}^{-1}$ level during the phase of velocity reversal. The Ti II line again appears to go through a slight slump just as δ Cep reaches maximum velocity. Surprisingly, the velocity of the high EP Si I and Mg I lines have a 0.7 km s^{-1} positive residual at phase 0.85. The Si II line has a negative velocity residual of 2 km s^{-1} relative to the standard Fe I lines.

For the case of η Aql (Fig. 12) and X Cyg (Fig. 13), all of the classes of lines except the Si II line have positive residual velocities of $2\text{--}5 \text{ km s}^{-1}$ during the phase of velocity reversal. The Si II line has a negative velocity residual of 3 and 5 km s^{-1} , respectively; for η Aql and X Cyg. The observation of X Cyg at phase 0.91 should be given very low weight. This observation was stopped early because of clouds, it has the lowest S/N of any observation taken in this project, and it was not possible to take a template observation (no iodine) of X Cyg at this phase because of the poor weather.

It is important to assess how the asymmetries of the line classes differ. Sasselov & Lester (1990) have defined an asymmetry parameter to describe the strength and direction of a line asymmetry. The position of the line core minimum is found by a parabolic fit to the three lowest points in the line. The location of the left and right half-height (midway between the continuum and the core) of the line is found by linear interpolation. The asymmetry parameter is given by the log of the ratio of the left half-width to the right half-width.

The asymmetry parameter as a function of phase for each of the program stars is shown in Figure 14. The crosses indicate the asymmetry parameter for the standard high EP Fe I lines, the diamonds represent the low EP Fe I, Fe II, Sc II, and Y II lines. All the lines follow a pattern of maximum left asymmetry near phase 0.0 and maximum right asymmetry near phase 0.8.

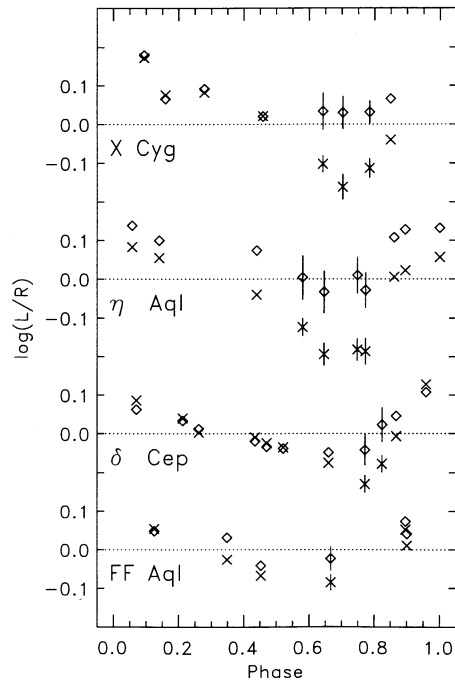


FIG. 14.—The Sasselov-Lester asymmetry parameter for each of the program stars. It is formed by taking the logarithm of the left-to-right half-width ratio of line profiles. Symmetric line profiles have a value of zero. Negative values indicate a blue extended line wing, positive for a red extended wing. The crosses represent the asymmetry for the standard high EP Fe I lines. The diamonds represent the lines of Sc II, Y II, Fe II, and the low EP lines of Fe I.

The maximum left asymmetry is similar for all the lines, but the maximum right asymmetry for the standard high EP Fe I lines is much greater than for the low EP lines. Though the EP of the Ti II lines is less than 2 eV, their asymmetry parameter is almost identical to the standard high EP Fe I lines. The 8.12 eV line of Si II also have an asymmetry parameter very similar to the standard Fe I lines. The high EP lines of Si I and Mg I have asymmetry parameters between the standard Fe I lines and the low EP lines. The asymmetry amplitude of the two larger amplitude Cepheids, η Aql and X Cyg, is significantly greater than the two smaller amplitude Cepheids.

7. DISCUSSION

In Eggen's Cepheid classification scheme, FF Aql is a type C Cepheid (Eggen 1985). Type C Cepheids are characterized by small amplitudes ($\leq 10 \text{ km s}^{-1}$), short periods, and sinusoidal velocity curves. With such small amplitudes, shocks play little or no role in these stars. Not surprisingly, line level effects are small in FF Aql. Velocity differences between various classes of lines differ at most by 0.5 km s^{-1} and line asymmetries differences are correspondingly small.

The three normal amplitude Cepheids in this study first show direct evidence of a radial velocity gradient just before the maximum infall velocity (near minimum light). The 8.12 eV line of Si II which is presumably formed near the continuum region is seen to undergo a negative velocity residual of $2\text{--}5 \text{ km s}^{-1}$ over a phase interval of 0.2–0.3, ending typically near minimum radius (phase $\cong 0.9$). This indicates that the Si II layer begins to slow while higher layers are still rapidly infalling. Similar behavior of the Si II line has been reported in SV

Vul (Grenfell & Wallerstein 1969) and X Cyg (Wallerstein 1983), but not in shorter period Cepheids (Wallerstein 1979; Jacobsen & Wallerstein 1981). The low EP lines of Fe I, Fe II, Ti II, Sc II, and Y II all show positive velocity residuals, typically peaking near minimum radius, suggesting that underlying layers have begun to move outward while the outer layers are still collapsing.

The problem of finding the actual velocity gradient of a Cepheid is compounded by line transfer. As Böhm-Vitense et al. (1989) point out, the optical layer from which a line is formed moves to deeper mass layers as the Cepheid expands and cools. From this hydrodynamic model, Karp (1975) has shown that measured velocity differences between optically thin and optically thick layers in Cepheids significantly underestimate the true velocity gradient. A future paper will attempt to disentangle the effects of line transfer and assign a depth of formation for each of the classes of lines discussed in this paper.

The observed IR asymmetry parameter given by Sasselov & Lester (1990, Fig. 15) for η Aql is nearly identical to that of the high EP Fe I lines shown in Figure 14. The asymmetry of these lines typically reach a maximum just before maximum infall velocity. One possible explanation for this is that the layer associated with the formation of the wings of the high EP lines is falling in faster than the layer in which the line core is formed, thus giving the lines a larger right half-width. The asymmetry of the low EP potential lines is much smaller than the high EP lines and is consistent with the model results of Sasselov & Lester (1990).

The determination of BE/BW distances and radii assume that the velocity curve of the continuum forming layer can be taken from the measured radial velocity curve. There are two serious problems with this assumption: (1) the measured velocity curve reflects motions in the outer line-forming layer of the atmosphere, and (2) the mass depth of the line-forming layer itself changes as the temperature and opacity of the Cepheid periodically change. The first problem leads to overestimating the radius change (and thus the distance) of a Cepheid. For example, the BE/BW distances derived for a handful of cluster Cepheids (Hindsley & Bell 1989) are typically 10%–20% larger than the previously determined cluster distances (Fernie & McGonegal 1983). To correct for this effect, Latyshev (1966) assumed the amplitude of the measured velocity curve is 10% larger than the continuum velocity curve. This is roughly consistent with the observed amplitude of the 8.12 eV line of Si II. The second problem leads to errors in finding the γ velocity. Oke et al. (1962) estimate that a 1 km s^{-1} error in deriving the γ velocity causes a 10% error in determining the BE/BW radii.

Ultimately the solution of these problems will require matching observations to a computer model of a hydrodynamic non-LTE atmosphere with radiative transfer and propagating shocks. The goal of such a code would be to match the observed velocity and asymmetry differences of various lines, as well as reproduce the overall light and velocity curves. It now appears that such a code could be working within the current decade (Sasselov & Raga 1992).

The author is indebted to R. A. Bell who originally suggested this project and has offered many insights. Heartfelt thanks are also due G. W. Marcy who has contributed an enormous amount of valuable advice and encouragement. The former Director of Lick Observatory, R. P. Kraft, was very generous in allocating observing time and facilities for this project.

Wayne Earthman built a critical exposure meter and provided observing and telescope support. The helpful comments of the referee, D. D. Sasselov, were appreciated. This research has

made use of the Simbad data base, operated at CDS, Strasbourg, France. The author gratefully acknowledges the support of a NASA Graduate Research Fellowship.

REFERENCES

- Abt, H. A. 1959, *ApJ*, 130, 769
 ———. 1978, *PASP*, 90, 309
 Baade, W. 1926, *Astron. Nach.*, 228, 359
 Barnes, T. G., Dominy, J. F., Evans, D. S., Kelton, P. W., Parsons, S. B., & Stover, R. J. 1977, *MNRAS*, 178, 661
 Barnes, T. G., Evans, D. S., & Parsons, S. B. 1976, *MNRAS*, 174, 503
 Barnes, T. G., Moffett, T. J., & Slovak, M. H. 1987, *ApJS*, 65, 307
 Beckers, J. M., Bridges, C. A., & Gilliam, L. B. 1976, *A High Resolution Spectral Atlas of the Solar Irradiance from 380 to 700 Nanometers* (Hanscom, Mass: Air Force Geophysics Laboratory)
 Bell, R. A. 1973, *MNRAS*, 164, 197
 Bell, R. A., & Rodgers, A. W. 1964, *MNRAS*, 128, 365
 Belopolsky, A. 1895, *ApJ*, 1, 160
 Böhm-Vitense, E., Garnavich, P., Lawler, M., Mena-Werth, J., Margan, S., Peterson, E., & Temple, S. 1989, *ApJ*, 343, 351
 Butler, R. P. 1992, *ApJ*, 394, L25
 Campbell, B. 1983, *PASP*, 95, 577
 Carroll, J. A. 1928, *MNRAS*, 88, 548
 Cochran, W. D., Hatzes, A. P., & Hancock, T. J. 1991, *ApJ*, 380, L35
 Eggen, O. J. 1985, *AJ*, 90, 1278
 Fernie, J. D. 1984, *ApJ*, 282, 641
 ———. 1992, in *IAU Colloq. 139, New Perspectives on Stellar Pulsations and Variable Stars*, in press
 Fernie, J. D., & McGonegal, R. 1983, *ApJ*, 275, 732
 Getting, I. E. 1935, *MNRAS*, 95, 141
 Gieren, W. 1981, *ApJS*, 46, 287
 Grenfell, T. C., & Wallerstein, G. 1969, *PASP*, 81, 732
 Griffin, R., & Griffin, R. 1973a, *MNRAS*, 162, 243
 ———. 1973b, *MNRAS*, 162, 255
 Hindsley, R., & Bell, R. A. 1986, *PASP*, 98, 881
 ———. 1989, *ApJ*, 341, 1004
 Jacobsen, T. S., & Wallerstein, G. 1981, *PASP*, 93, 481
 Joy, A. H. 1939, *Mt. Wilson Contrib.*, 607
 Karp, A. H. 1975, *ApJ*, 201, 641
 Kraft, R. P. 1956, *PASP*, 68, 137
 ———. 1967, in *IAU Symp. 28, Aerodynamic Phenomena in Stellar Atmospheres*, ed. R. N. Thomas (New York: Academic), 207
 Kulander, J. L., & Jefferies, J. T. 1966, *ApJ*, 146, 194
 Latyshev, I. N. 1966, *Astrophysica*, 2, 355
 Manduca, A., & Bell, R. A. 1981, *ApJ*, 250, 306
 Marcy, G. W., & Butler, R. P. 1992, *PASP*, 104, 270
 McMillan, R. S., Moore, T. L., Perry, M. L., & Smith, P. H. 1993, *ApJ*, 403, 801
 Merline, W. J. 1985, in *IAU Colloq. 88, Stellar Radial Velocities*, ed. A. G. Davis Philip & D. W. Latham (Schenectady: L. Davis), 87
 Moore, C. E., Minnaert, M., & Houtgast, J. 1966, *The Solar Spectrum 2935 Å to 8770 Å* (NBS Monograph 61)
 Nadeau, D., & Maillard, J. P. 1988, *ApJ*, 327, 321
 Oke, J. B., Giver, L. P., & Searle, L. 1962, *ApJ*, 136, 393
 Parsons, S. B. 1971, *MNRAS*, 152, 121
 ———. 1972, *ApJ*, 174, 57
 Rodgers, A. W., & Bell, R. A. 1964, *MNRAS*, 127, 471
 Sanford, R. F. 1952, *ApJ*, 116, 331
 ———. 1956, *ApJ*, 123, 201
 Sasselov, D. D., & Lester, J. B. 1990, *ApJ*, 362, 333
 Sasselov, D. D., Lester, J. B., & Fieldus, M. S. 1989, *ApJ*, 337, L29
 Sasselov, D. D., & Raga, A. 1992, in *The Seventh Cambridge Workshop on Cool Stars, Stellar Systems, and the Sun*, ed. M. S. Giampapa & J. A. Bookbinder (ASP Conf. Ser., 26), 549
 Shane, W. W. 1958, *ApJ*, 127, 573
 Vogt, S. S. 1987, *PASP*, 99, 1214
 Wallerstein, G. 1972, *PASP*, 84, 656
 ———. 1979, *PASP*, 91, 772
 ———. 1983, *PASP*, 95, 422
 Wesselink, A. J. 1946, *Bull. Astron. Inst. Netherlands*, 10, 91
 ———. 1969, *MNRAS*, 144, 297